Ore Geology Reviews 112 (2019) 103010

Contents lists available at ScienceDirect

Ore Geology Reviews

journal homepage: www.elsevier.com/locate/oregeorev

The continental crust contributes to magmatic hydrothermal gold deposit in Ciemas, West Java, Indonesia: Constraints from Hf isotopes of zircons and *in situ* Pb isotopes of sulfides

Chengquan Wu[a,*], Zhengwei Zhang[a,*], Mega Fatimah Rosana[c], Qiao Shu[a], Chaofei Zheng[a,b], Jinhong Xu[a,b], Xiyao Li[a,b], Ziru Jin[a,b]

[a] State Key Laboratory of Ore Deposit Geochemistry, Institute of Geochemistry, Chinese Academy of Sciences, Guiyang 550081, China
[b] University of Chinese Academy of Sciences, Beijing 100049, China
[c] Faculty of Geology, University of Padjadjaran, Jln. Raya Bandung – Sumedang Km. 21, Jatinangor, Sumedang 45363, Indonesia

ARTICLE INFO

Keywords:
Hf isotope
In situ Pb isotope
Porphyry-epithermal mineralization
Magmatic origin
West Java, Indonesia

ABSTRACT

Multiple periods of arc magmatism induced by the subduction of the Indian-Australian Plate northward developed on Java Island, and multistage porphyry-epithermal metallogenic systems occurred within the Late Eocene-Early Miocene and the Late Miocene-Early Pleistocene magmatic belts. These porphyry-epithermal metallogenic systems have obvious spatial variations. In West Java, there are large populations of low-sulfidation type epithermal deposits, while East Java and its east are characterized by the occurrences of porphyry deposits. However, the newly discovered Ciemas deposit in West Java, a Middle Miocene (~17 Ma) porphyry-epithermal Au deposit, provides an opportunity for further understanding the porphyry-epithermal mineralization in Java. To elucidate the controlling factors of porphyry-epithermal mineralization in West Java, we analyzed the Hf isotopies of zircons from the igneous rocks and *in situ* Pb isotopes of sulfides (galena, pyrite, arsenopyrite) in the Ciemas deposit. The results show that the zircons $\varepsilon_{Hf}(t)$ of igneous rocks are uniform with an average value of -11.5 ± 0.39, and the peak value of T_{DM2} is 1500–1650 Ma, suggesting the Middle Miocene arc magmatism in Ciemas suffered intense crustal contamination. The Pb isotopic compositions of sulfides are very uniform and have high amounts of radiogenic lead. The mean ratios of $^{206}Pb/^{204}Pb$, $^{207}Pb/^{204}Pb$ and $^{208}Pb/^{204}Pb$ are 39.343 ± 0.059, 15.73 ± 0.015 and 18.854 ± 0.025, respectively, indicating that the mineralization materials of the Ciemas gold deposit mainly originated from ancient continental crust. The multistage arc magmatism induced by the subduction of the Indian-Australian Plate northward beneath Java Island control the porphyry and epithermal mineralization in Java. The Middle Miocene arc magmatism in Ciemas contaminated intensely by the Sundaland, and the ancient continental crust provides the main metal source for the Ciemas deposit in West Java.

1. Introduction

Java Island is located in the subduction zone between the Indian-Australian Plate and the Eurasian Plate (Fig. 1A) (Bemmelen, 1949, 1970). The Indian-Australian Plate has drifted northward since the Mesozoic and has been subducted beneath the Eurasian Plate since the Eocene (Katili, 1975; Hamilton, 1979). Multiple periods of magmatic activities induced by the subduction occurred in the subduction zone, which formed the Sunda-Banda Arc (Katili, 1975). This arc extends from the north of Sumatra, through Java, and continues to Banda Islands (Fig. 1A) (Hamilton, 1979). Java Island is located in the middle of the Sunda-Banda Arc, where there are multiple stages of arc magmatism (Fig. 1) (Bemmelen, 1949, 1970; Katili, 1975; Whitford et al., 1979; Soeria-Atmadja et al., 1994). Correspondingly, multistage porphyry-epithermal gold (silver) copper mineralization systems developed in these arc magmatic belts, including Cibaliung Au (Ag), Pongkor Au-Ag, Ciemas Au and Tumpangpitu Cu-Au deposits (Harijoko et al., 2004; Rosana et al., 2006; Harijoko et al., 2007; Imai and Watanabe, 2007; Warmada et al., 2007; Wu et al., 2015; Zhang et al., 2015; Zheng et al., 2017; Harrison et al., 2018). Furthermore, plate subduction throughout Java and the associated volcanism and porphyry-epithermal mineralization continue to this day (Setijadji et al., 2006). Therefore, Java Island is an ideal area for studying plate subduction and the associated porphyry-epithermal mineralization (Milési et al., 1994; Warmada

* Corresponding authors.
E-mail addresses: wuchengquan@mail.gyig.ac.cn (C. Wu), zhangzhengwei@vip.gyig.ac.cn (Z. Zhang).

https://doi.org/10.1016/j.oregeorev.2019.103010
Received 7 March 2019; Received in revised form 17 June 2019; Accepted 8 July 2019
Available online 20 July 2019

et al., 2007; Yuningsih et al., 2014; Zhang et al., 2015; Maryono et al., 2018).

The porphyry-epithermal metallogenic systems in Java have obvious spatial variations (Fig. 1B). In West Java, there are large populations of low-sulfidation type epithermal deposits and few porphyry deposits and the metallogenic element assemblages are dominated by Au-Ag-Pb-Zn (Marcoux and Milési, 1994; Yuningsih et al., 2014; Zhang et al., 2015), while East Java and its east are characterized by the occurrences of porphyry deposits and the metallogenic element assemblages are mainly Cu-Au (Yuningsih et al., 2014; Harrison et al., 2018; Maryono et al., 2018). The low-sulfidation epithermal deposits in West Java are mainly occurred within the Bayah Dome (Fig. 1B) (Marcoux et al., 1993; Basuki et al., 1994; Marcoux and Milési, 1994; Milési et al., 1994; Milési et al., 1999). Some mineralizations related to the Jampang Formation have been gradually regarded (Setijadji et al., 2006; Zhang et al., 2015). Previous studies on mineralization in West Java were mostly focused on Bayah Dome, Simpenan, Cisolok -Sukabumi, Cupunagara-Subang, Gunung Subang, Tanggeung-Cianjur, Cijulang-Pangalengan and Cineam-Tasikmalaya (Marcoux and Milési, 1994; Milési et al., 1994; Widi and Matsueda, 1998; Indarto et al., 2006; Ismayanto et al., 2007; Sunarie et al., 2009; Kisman, 2011; Tun et al., 2014; Yuningsih et al., 2014; Prabowo et al., 2018). The oldest deposit previously found in West Java (low-sulfidation Cibaliung Au-Ag deposit) formed in 11.18–10.65 Ma (Angeles et al., 2002; Harijoko et al., 2004; Harijoko et al., 2007). The discovery of the Ciemas Deposit in West Java, a Middle Miocene (~17 Ma) porphyry-epithermal Au deposit, advances the previous understanding of porphyry-epithermal mineralization in Java (Wu et al., 2014, 2015; Zhang et al., 2015; C. F. Zheng et al., 2014a, 2014b; Zheng et al., 2017).

The Ciemas deposit, located in the south of westernmost Java (Fig. 1B), is a recently discovered porphyry-epithermal Au deposit (Wu et al., 2014; Wu et al., 2015; Zhang et al., 2015; Zheng et al., 2017), which provides an opportunity for further understanding the porphyry-epithermal mineralization in Java. The ore deposit geology and the elemental geochemistry of the associated igneous rocks have been described in detail (Wu et al., 2014; Wu et al., 2015; Zhang et al., 2015; Zheng et al., 2017). However, the origins of metallogenic magma and ore-forming materials is still unclear. This paper analyzes the Hf isotopies of zircons from the Middle Miocene igneous rocks and *in situ* Pb isotopes of sulfides (galena, pyrite, arsenopyrite) in the Ciemas deposit, which is useful for understanding the origins of magmatism and the ore-forming material in Ciemas and elucidating the controlling factors of porphyry-epithermal mineralization in West Java.

2. Geological background

Java is located on the southeastern edge of the Eurasian Plate, where tectonics are very active and earthquakes and volcanism caused by subduction are frequent (Fig. 1A) (Bemmelen, 1949, 1970). West Java is located at the southern boundary of Sundaland (Fig. 1A). The Sundaland is the continental core of Southeast Asia (Fig. 1A) (Hall, 2002; Clements and Hall, 2007; Hall et al., 2008). However, East Java is

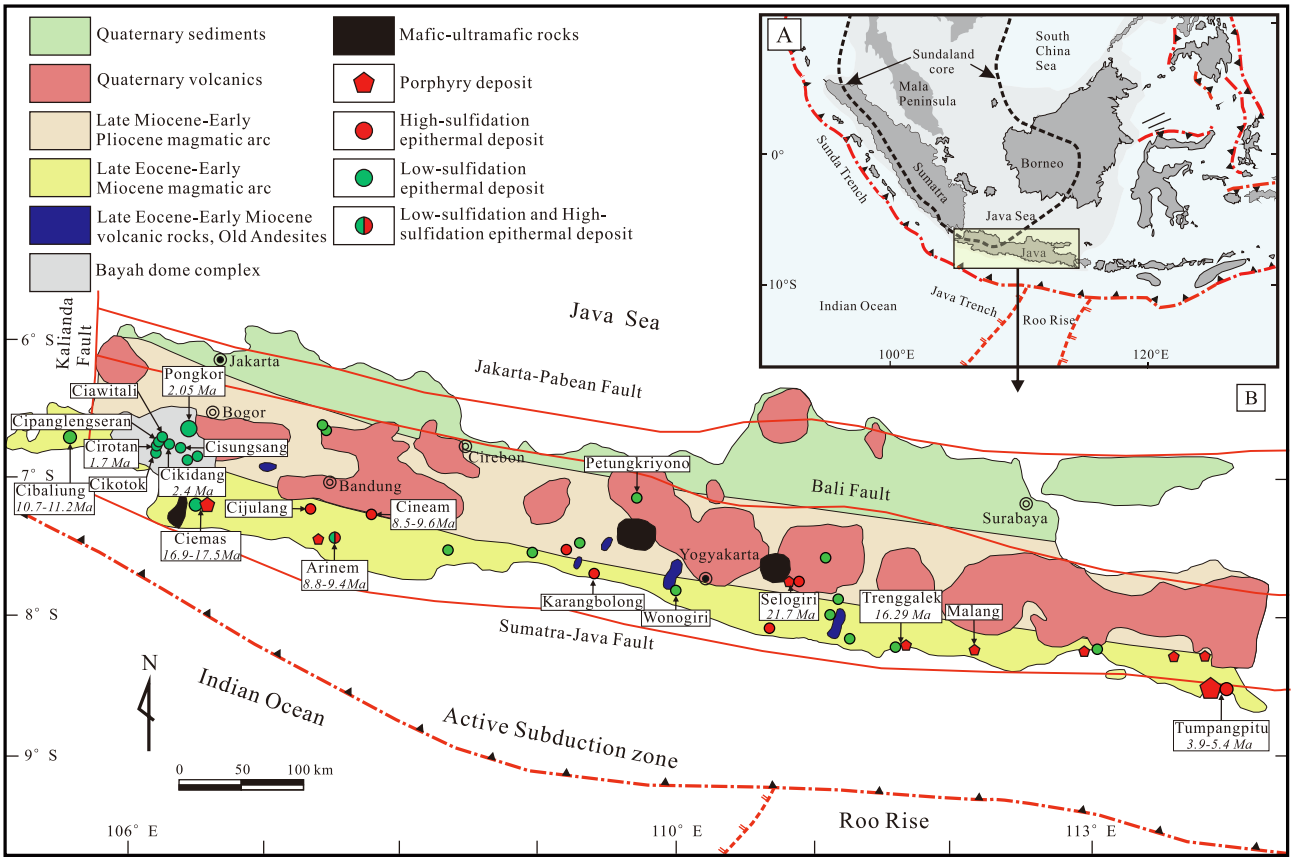

Fig. 1. A-Tectonic diagram of Java Island (modified from (Hall, 2002; Hall et al., 2008)): B-Geological map and distributions of metal deposits on Java Island (modified from (Carlile and Mitchell, 1994; Soeria-Atmadja et al., 1994; Rosana and Matsueda, 2002a; Rosana and Matsueda, 2002b; Harijoko et al., 2004; Rosana et al., 2006; Setijadji et al., 2006; Harrison et al., 2018; Maryono et al., 2018)).

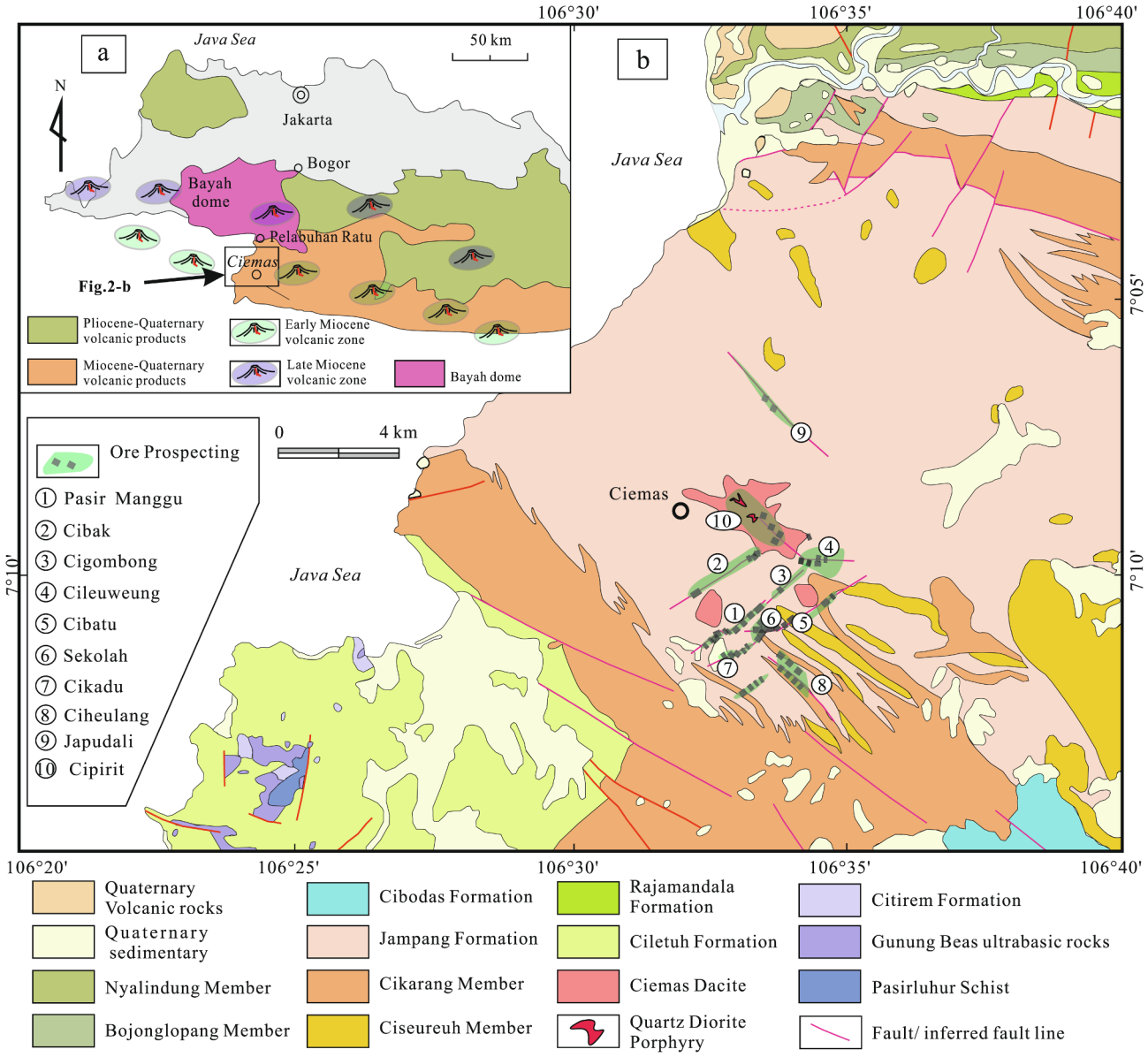

Fig. 2. Diagram of West Java showing the location of the Ciemas deposit (a). Geological map of Ciemas Au deposit, West Java, Indonesia (b) (modified from (Sukamto, 1975; Milési et al., 1999; Jonathan, 2007; Zhang et al., 2015)).

mainly an accretionary crust, which was formed by the arc magmatism induced by the subduction of the Indian-Australian Plate since the Eocene (Fig. 1A) (Katili, 1975; Hamilton, 1979).

The exposed strata in Java are mainly Tertiary and Quaternary (Fig. 1B) (Hamilton, 1979). Tertiary and Quaternary pyroclastic rocks are mainly distributed in southern and central part of Java. These rocks are mainly rhyolitic, dacitic-andesitic tuff, breccia and lava and are partially intercalated with sandstone, shale, carbonaceous tuff and mudstone. The Quaternary sediments are dominant in northern Java (Fig. 1B) (Hamilton, 1979; Wakita and Metcalfe, 2005). In the Ciemas area, most exposed rocks are Tertiary volcanics and Quaternary residual deposits (Fig. 1B) (Sukamto, 1975; Zhang et al., 2015).

Java Island is located to the north of the Java trench. The Sumatran-Java Trench runs in the NW-EW direction, with a total length of over 4880 km (Fig. 1A) (Hamilton, 1989). The subduction along Sumatra is oblique and that along Java is orthogonal (Malod et al., 1995). The faults in Java trend mainly EW and NS, including the middle segment of the Sumatra-Java Fault, the Jakarta-Pabean Fault, the western segment of the Bali Fault and the southern segment of the Kalianda Fault (Fig. 1B) (Hamilton, 1973; Katili, 1975; Hamilton, 1979).

The magmatism that occurred in Java was mainly in the Cenozoic (Katili, 1975). From south to north are the Late Eocene-Early Miocene magmatic belt (40 Ma to 19–18 Ma) in southern Java, the Late Miocene-Early Pleistocene belt (12 or 11 Ma to 2 Ma) in central Java, and the Quaternary belt in north-central Java (Fig. 1B) (Nicholls et al., 1980; Soeria-Atmadja et al., 1994; Yao et al., 2010). Ciemas is located within

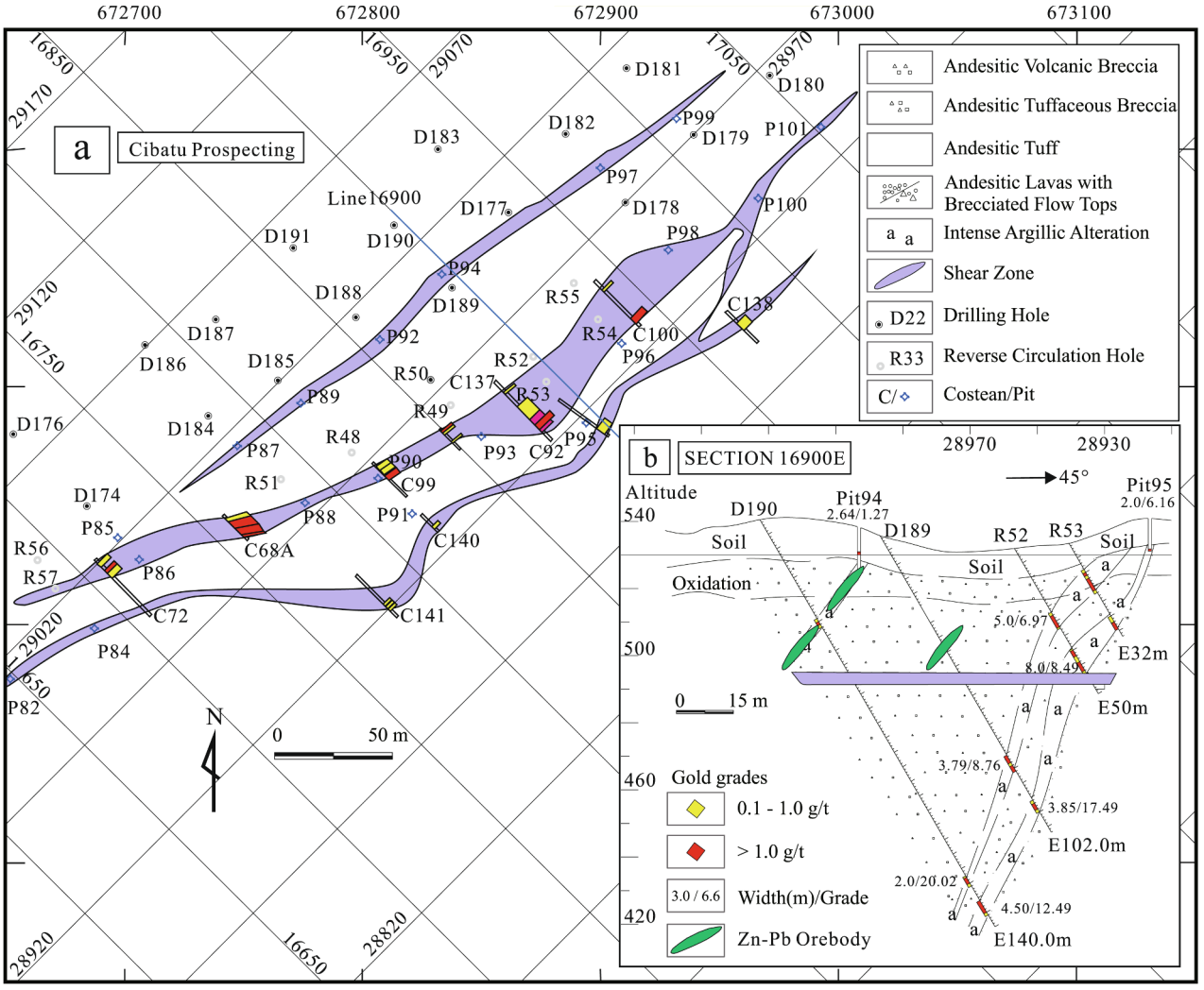

Fig. 3. Geological map of the Cibatu ore block (a) and section map of the 16900E prospecting line in the Ciemas gold deposit (b) (modified form (Jonathan, 2007; Zhang et al., 2015)).

the Late Eocene-Early Miocene belt (Fig. 1B) (Wu et al., 2015). A Middle Miocene quartz diorite porphyry intruded into the dacite and andesite in Ciemas (Fig. 2B) (Wu et al., 2015; Zhang et al., 2015).

3. Deposit descriptions

Ciemas is a porphyry-epithermal type gold deposit that is associated with Miocene quartz diorite porphyry, dacite and andesite (Zhang et al., 2015; C. F. Zheng et al., 2014a, 2014b; Zheng et al., 2017). Three ore types have been identified as porphyry, quartz-sulfide veins, and structure-controlled alteration rocks. Ten ore blocks have been discovered (Fig. 2B), and the Pasir Manggu, Cigombong, Cileuweung and Cibak are quartz vein ore blocks, the Ciheulang, Cibatu, Cikadu, Sekolah and Japudali are structure-controlled alternated ore blocks, and the Cipirit is a porphyry ore block (Zhang et al., 2015).

The ore bodies of the quartz-sulfide veins and structure-controlled types mainly occur within the dacite and fracture zones and are shaped as veins and layered veins, and are mostly NW-trending, with some SE-trending, dipping 70–80° to the east (Wu et al., 2014; Zhang et al., 2015). The major ore bodies are generally several hundreds of meters long, with thicknesses of up to a few meters (Fig. 3). The Au reserves measured and indicated from Pasir Manggu, Cibatu, Cikadu, and Sekolah ore blocks are 26.74 t, with an average grade of 8.8 g/t. The inferred Au resources are 12.23 t with an average grade of 7.6 g/t (Zhang et al., 2015; Zheng et al., 2017).

In the Cipirit block, a porphyry intrusion has been identified (Wu et al., 2014). The exposed intrusion is a quartz diorite porphyry with more than 2000 m long and about 500 m wide (Fig. 4a). The quartz diorite porphyry intruded into Miocene dacite and andesite and is covered by a weathering and argillaceous alteration zone (Fig. 5a–b) (Wu et al., 2015). The intrusion mainly contain coarse-grained quartz diorite porphyry (Fig. 4b). Some fine- to medium-grained porphyry veins occurred surrounding and inside the intrusion (Fig. 4b). The porphyry is grayish white in colour (Fig. 5c and d). The rock has a massive structure and porphyritic texture, with quartz and hornblende phenocrysts (Fig. 5d–e), and the matrix is mainly cryptocrystalline quartz and feldspar (Fig. 5e). Quartz phenocrysts are coarse-grained, and the hornblende phenocrysts are columnar in shape (Fig. 5d–e). The

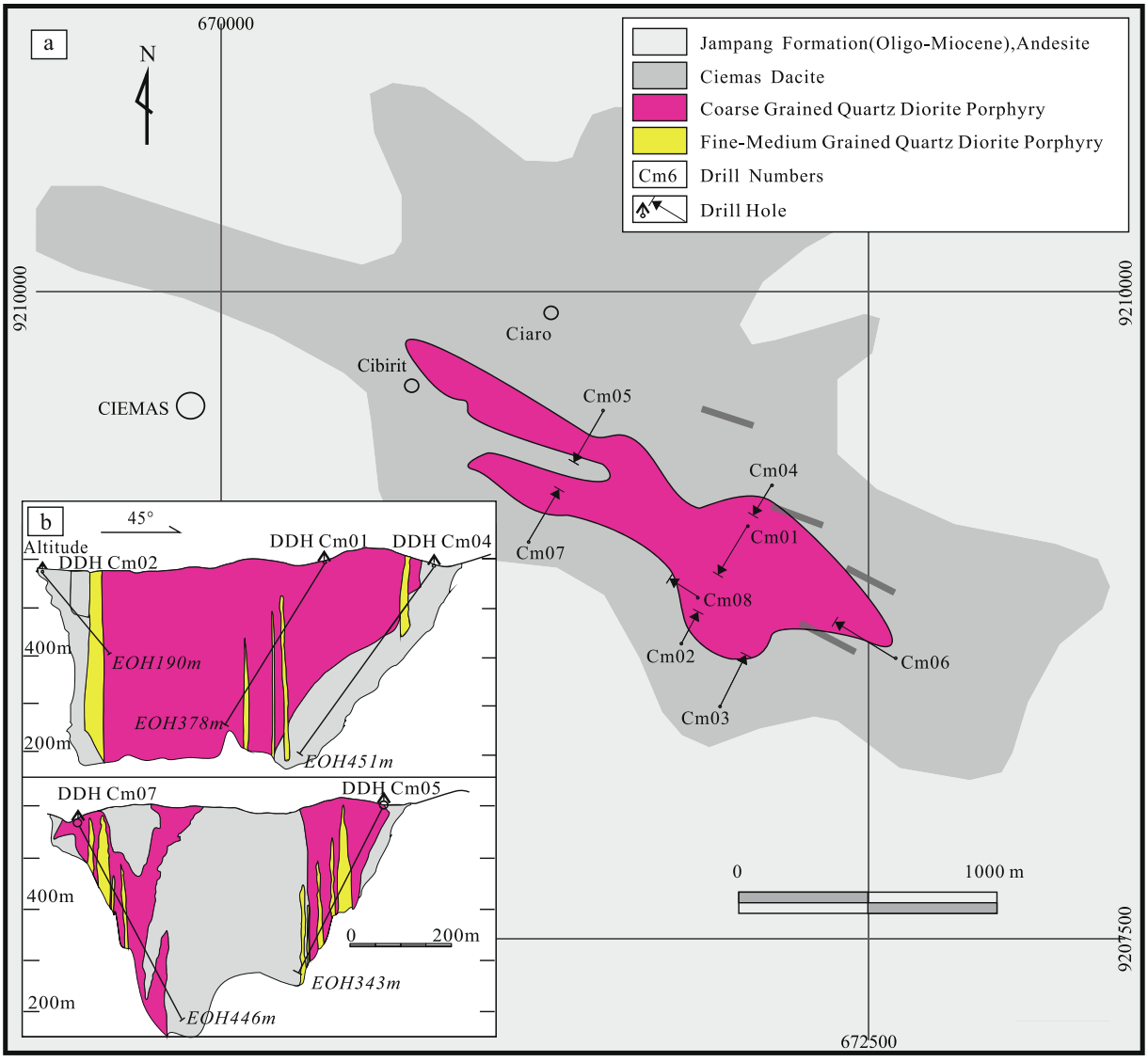

Fig. 4. Section map of the quartz diorite porphyry intrusion in Ciemas (modified after (Wu et al., 2015; Zhang et al., 2015));

pyrite and chalcopyrite mineralization occur within the quartz diorite porphyry (Fig. 4f). The ore body occurred as discontinuous layer and vein in structure. The length of ore body is 20–80 m with a thickness of 3–10 m. The inferred Au resource is 19.91 t @1.2 g/t (Zhang et al., 2015).

The ore minerals are mainly pyrite, arsenopyrite, galena, sphalerite and chalcopyrite (Fig. 6). The gangue minerals are mainly composed of quartz, plagioclase, chlorite, sericite and calcite. The textures of ores include metasomatic (Figs. 6A, B, E and H), euhedral–subhedral granular (Figs. 6C, D, G and I), poikilitic (Fig. 6F), columnar and metasomatic relict. The ore structures are mainly disseminated, brecciated, veinlet and massive.

The wall rock alteration types are mainly potassic, argillic, pyritization, chloritization, epidotization, silicification and carbonatization. The thickness of the alteration zones reach as much as 5 m at the top of the ore body but become narrower at the footwall. The clay minerals consist of kaolinite, smectite and illite.

4. Analytical methods and results

4.1. Analytical methods

The zircons were selected from the quartz diorite porphyry, andesite and amphibolic tuff breccia in Ciemas. The detailed geochemistry and zircon U-Pb dating of these igneous rocks were described in (Wu et al., 2015; Zhang et al., 2015). Sulfides from the Cipirit porphyry ore block, Cibatu structure-controlled alternated ore block, Pasir Manggu and Cibak quartz vein ore blocks were selected to analyze the in situ Pb isotopes.

Experiments analyzing the in situ Hf isotopic ratio of zircons were conducted at the Wuhan Sample Solution Analytical Technology Co., Ltd, Hubei, China, using a Neptune Plus MC-ICP-MS in combination with Geolas HD excimer ArF laser ablation. Helium was used as the carrier gas within the ablation cell and was merged with argon after the ablation cell. Small amounts of nitrogen were added to the argon

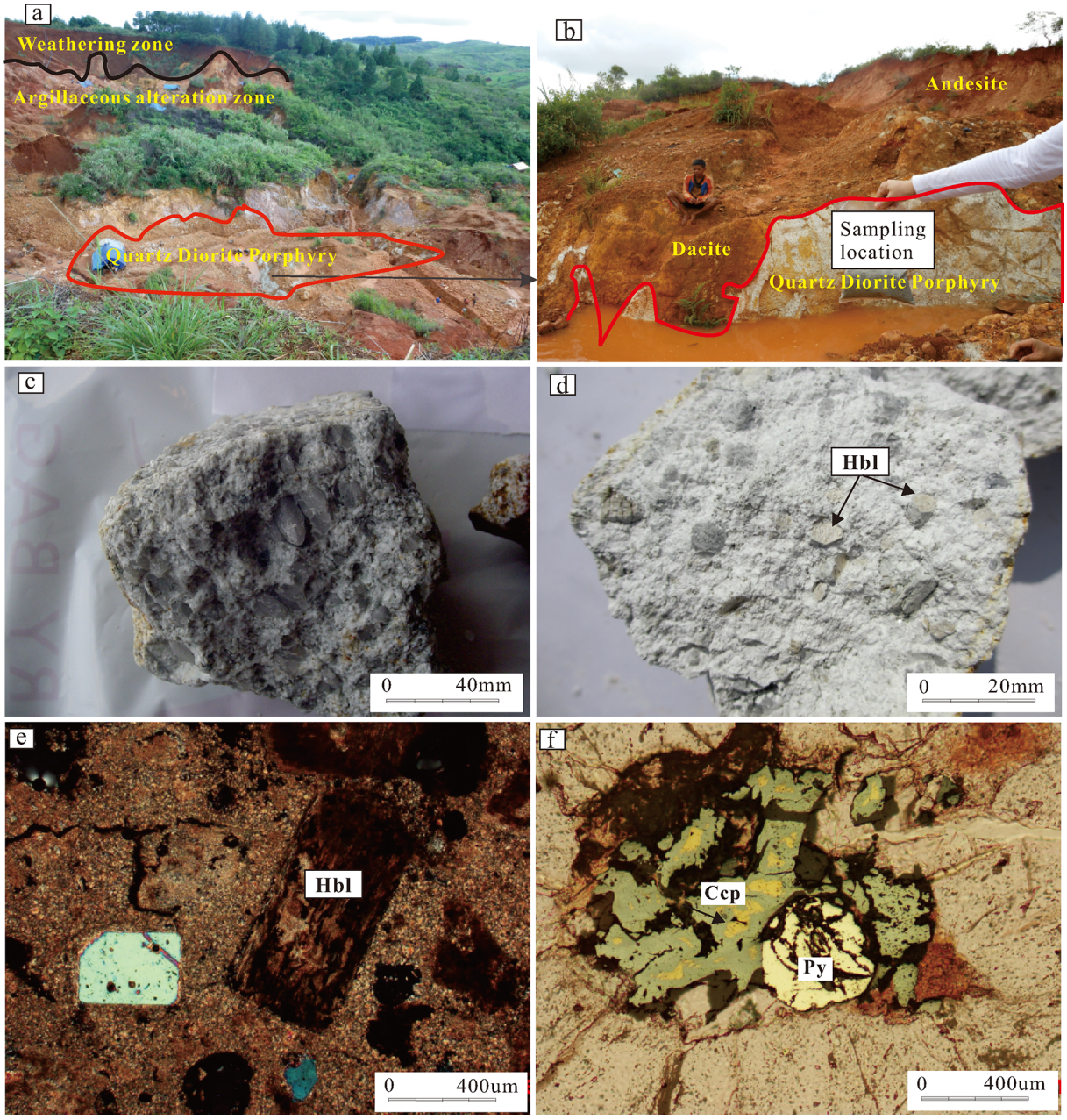

Fig. 5. (a) exposed quartz diorite porphyry; (b) quartz diorite porphyry intruded into andesite and dacite; (c) quartz diorite porphyry is of massive structure and porphyritic texture; (d) columnar hornblende phenocryst; (e) columnar hornblende phenocryst; the matrix is mainly cryptocrystalline quartz and feldspar (cross-polarized light); (f) chalcopyrite and pyrite occurred in the porphyry (reflected light). Hbl-hornblende, Py-pyrite, Ccp-chalcopyrite.

makeup gas flow to improve the sensitivity of Hf isotopes (Hu et al., 2012a; Hu et al., 2012b). All data were acquired on zircon in single spot ablation mode at a spot size of 44 μm. The energy density of laser ablation was ~7.0 J/cm. Each measurement consisted of 20 s of acquisition of the background signal followed by 50 s of ablation signal acquisition. The details of method are available in (Hu et al., 2012a). The data processing was performed by ICPMSDataCal (Liu et al., 2010).

In situ Pb isotope analyses were conducted by a RESOlution M-50 laser ablation system (ASI, Australia), connected to a Nu Plasma II MC-ICP-MS from Nu Instruments (Wrexham, UK) at the State Key Laboratory of Continental Dynamics, Northwest University, Xi'an. Helium was used as a carrier gas at an uptake rate of 280 mL/min, with a 6 Hz repetition time and 6 J/cm^2 energy density during the laser ablation process. The laser ablation beam diameter was 9 μm for galena and 100 μm for the other sulfides. Each analysis consisted of a background measurement for 30 s, followed by 50 s of ablation for signal collection and an additional 40 s of washing time. The PSPT-2, Gn01, and NIST SRM 610 glass served as internal and external standards,

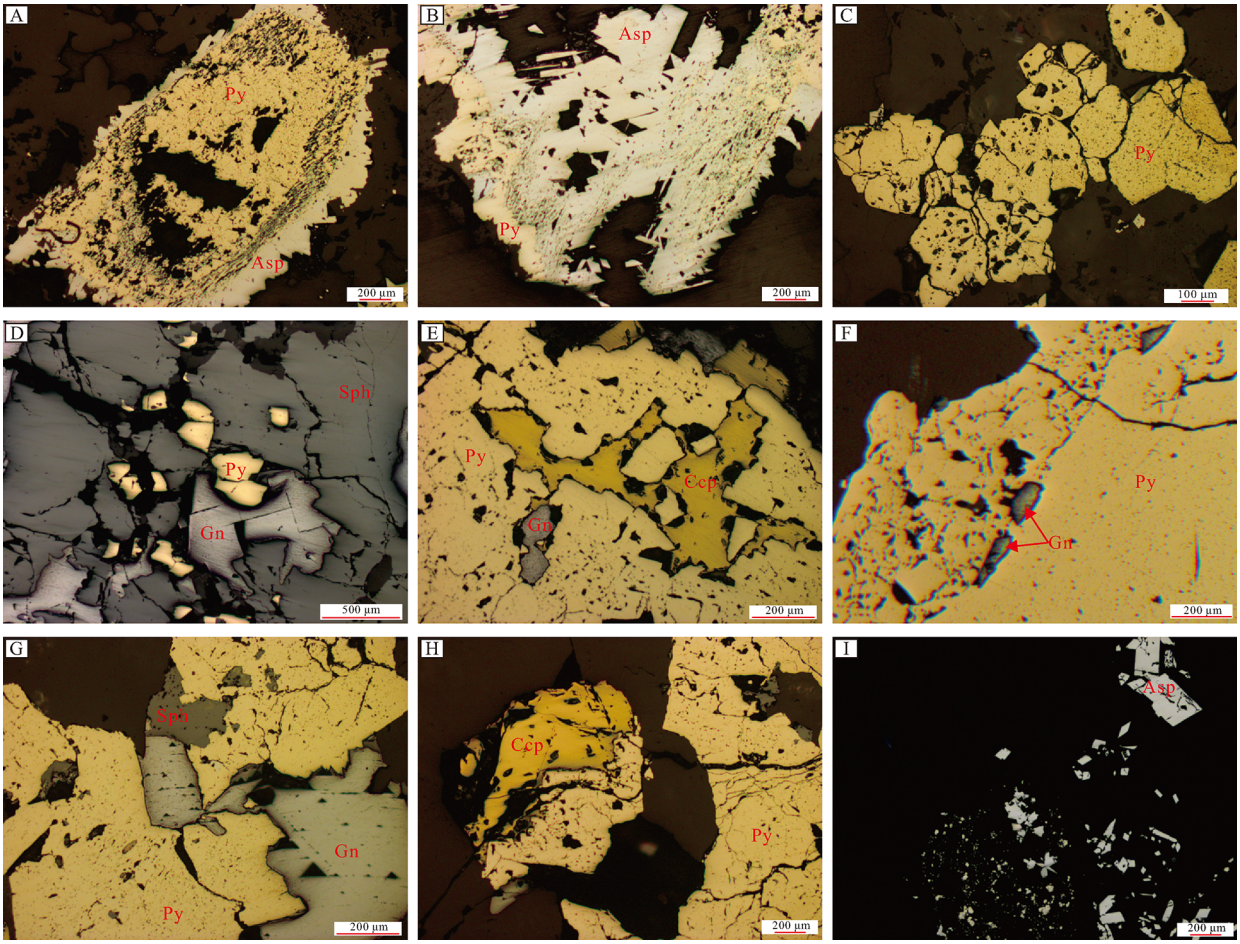

Fig. 6. Micrographs of ore minerals from the Ciemas gold deposit. A, B, C are from the Cibak quartz vein ore block; A and B: metasomatic texture with pyrite replaced by arsenopyrite; C: subhedral granular pyrite; D, E, F are from the structure-controlled alternated Cibatu ore block; D: symbiotic pyrite, galena and sphalerite; E: metasomatic texture with pyrite replaced by chalcopyrite; F: poikilitic texture with galena encased in pyrite; G, H, I are from Pasir Manggu quartz vein ore block; G: symbiotic pyrite, galena and sphalerite; H: metasomatic texture with pyrite replaced by chalcopyrite; I: euhedral granular arsenopyrite. Py-pyrite, Asp-arsenopyrite, Gn-galena, Sph-sphalerite, Ccp-chalcopyrite.

respectively. The measured isotopic ratios of these standards were highly reliable and reproducible and yielded agreement with the references during the analytical process (Yuan et al., 2018). The details of the fs LA-MC-ICP-MS *in situ* Pb isotope analysis and instrument parameters are available in (Bao et al., 2017).

4.2. Results

The cathode luminescence (CL) images of representative zircons analyzed for *in situ* U-Pb and Hf isotopes of igneous rocks in Ciemas are shown in Fig. 7. The quartz diorite porphyry, andesite, and amphibolic tuff breccia yielded 17.1 ± 0.4 Ma (Fig. 8a), 17.5 ± 0.3 Ma) (Fig. 8b) and 16.9 ± 0.3 Ma (Fig. 8c), respectively (Wu et al., 2015).

The zircons εHf (*t*) of the quartz diorite porphyry is −12.3 to −9.1 (average = −10.94 ± 0.67, n = 12) (Fig. 9a), that of the andesite is −13.7 to −9.9 (average = −11.70 ± 0.61, n = 15) (Fig. 9b) and that of the amphibolic tuff breccia is −13.7 to −8.1 (average = −10.80 ± 0.78, n = 17) (Fig. 9a and Table 1). All the εHf (*t*) values of these samples are similar, with an average of −11.15 ± 0.39 (Fig. 9d).

The calculated two-stage model age (T_{DM2}) of the quartz diorite porphyry is 1449–1647 Ma (average = 1572 Ma), that of the andesite is 1515–1720 Ma (average = 1615 Ma) and that of the amphibolic tuff breccia is 1415–1723 Ma (average = 1563 Ma) (Table 1).

The results of Pb isotopic compositions of sulfides in Ciemas are shown in Table 2. The Pb contents of pyrite from the Cipirit ore block are too low, which resulted in unavailable Pb isotopic compositions. In the Cibak ore block, the average ratios of $^{206}Pb/^{204}Pb$, $^{207}Pb/^{204}Pb$ and $^{208}Pb/^{204}Pb$ from pyrite are 18.847 ± 0.035, 15.732 ± 0.025 and 39.348 ± 0.064, respectively, and those from arsenopyrite are 18.828 ± 0.018, 15.721 ± 0.01 and 39.283 ± 0.065, respectively. In the Pasir Manggu ore block, the average ratios of $^{206}Pb/^{204}Pb$, $^{207}Pb/^{204}Pb$ and $^{208}Pb/^{204}Pb$ from galena are 18.869 ± 0.007, 15.733 ± 0.005 and 39.380 ± 0.017, respectively, and those from pyrite are 18.864 ± 0.007, 15.73 ± 0.008 and 39.377 ± 0.018, respectively. In the Cibatu ore block, the average ratios of $^{206}Pb/^{204}Pb$, $^{207}Pb/^{204}Pb$ and $^{208}Pb/^{204}Pb$ from galena are 18.873 ± 0.004, 15.736 ± 0.004 and 39.374 ± 0.024, respectively, and those from pyrite are 18.860 ± 0.007, 15.726 ± 0.007 and 39.351 ± 0.018, respectively (see Fig. 11.).

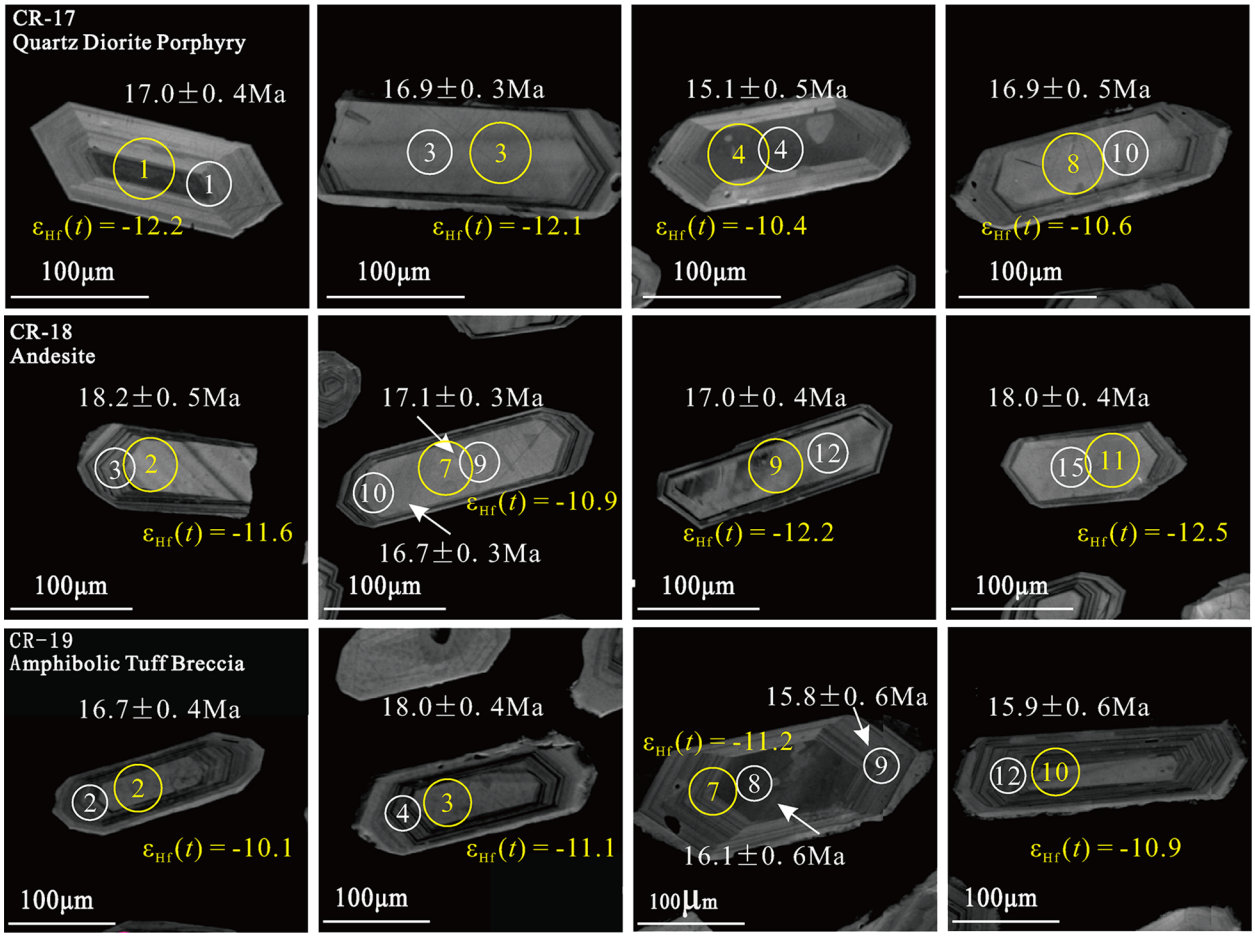

Fig. 7. Cathode luminescence (CL) images of representative zircons analyzed for *in situ* U-Pb and Hf isotopes of quartz diorite porphyry, andesite, and amphibolic tuff breccia in Ciemas.

5. Discussion

5.1. Origins of magmatism and continental contamination

Java is located in the southern border of Sundaland (Fig. 1B). The Sundaland is the core of the mainland of Southeast Asia and was accreted in the Late Cretaceous (Bemmelen, 1970). The basement of Sundaland mainly contains Paleozoic-Mesozoic granite and metamorphic rocks (Audley-Charles et al., 1988; Metcalfe, 1996). In the Late Cretaceous, a terrane from Gondwanaland accreted to Java and Sulawesi (Smyth et al., 2007). A subduction zone formed southwest of Sulawesi as the Indian-Australian Plate subducted beneath the Eurasian Plate (Katili, 1978). The Sunda Arc formed along the northern border of this active convergence and has been active since the Eocene (Hamilton, 1973; Katili, 1975; Hamilton, 1979). Multiple periods magmatism related to the subduction zone occurred in the Java Island (Soeria-Atmadja et al., 1994).

The Sumatra-Java metallogenic belt is divided into Sumatra and Java segments, both of which are located in the western part of the Sunda-Banda Arc (Fig. 1A) (Carlile and Mitchell, 1994; Yao et al., 2010). The crust underneath the Sunda Arc thins eastward, from approximately 30 km beneath the Sumatra to 15 km beneath the Flores Sea. The thickness of crust is approximately 20–25 km beneath Java (Ben-Avraham and Emery, 1973). In West Java, the basement of the crust is the Sundaland, which is similar to that of Sumatra (Hamilton, 1979; Setijadji et al., 2006), while East Java is above on an island arc crust, starting from the Cretaceous accretionary complex in central Java to principally oceanic crust further east (Carlile and Mitchell, 1994; Miyazaki et al., 1998; Setijadji et al., 2006; Smyth et al., 2007).

Therefore, the arc magmatism is obviously different in Java due to the different underlying basement. West Java is located above the Sundaland, and the magmatism is easily contaminated by the ancient continental crust (Marcoux and Milési, 1994), while East Java mainly lies above the oceanic crust, where the magmatism shows more mantle affinity without or less continental participation (Elburg et al., 2004; Setijadji et al., 2006).

Based on K-Ar dating, the magmatism in Java can be divided into three belts, which trend to become younger from south to north: Late Eocene to Early Miocene (40 to 19–18 Ma), Late Miocene to Pliocene (12 or 11–2 Ma), and Quaternary (Fig. 1B) (Soeria-Atmadja et al., 1994). The Late Eocene to Early Miocene belt was emplaced along the southern part of Java, trending from west to east. The Late Miocene to Pliocene belt occurred further north, parallel to the older belt and in places is overlain by Quaternary volcanic rocks (Fig. 1B) (Soeria-Atmadja et al., 1994).

The Ciemas deposit is within the Late Eocene to Early Miocene

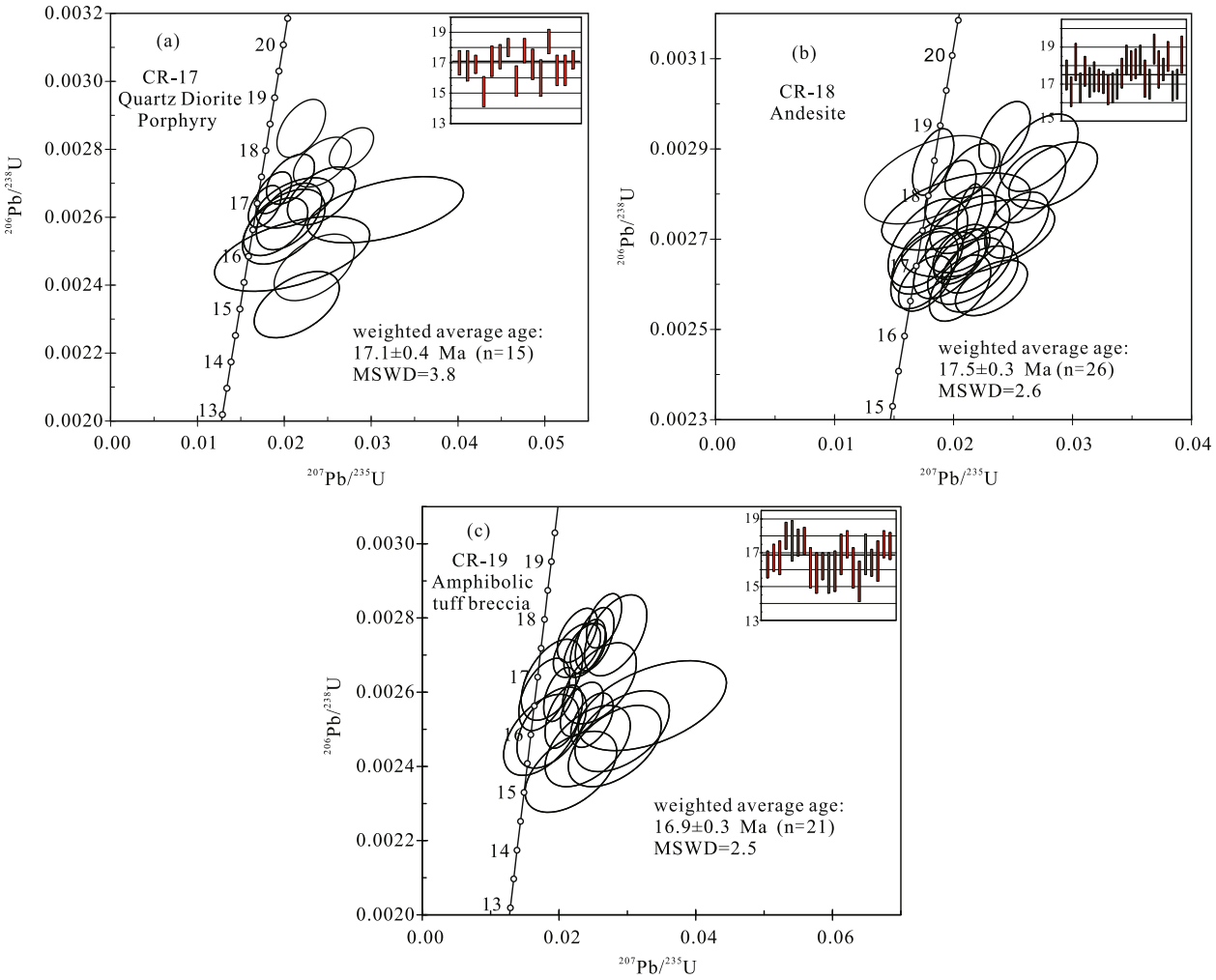

Fig. 8. Zircon U-Pb concordia diagram of quartz diorite porphyry (a), andesite (b), and amphibolic tuff breccia (c) in Ciemas (after (Wu et al., 2015)).

magmatic belt (Fig. 1B). The U- Pb zircon ages of the quartz diorite porphyry, andesite, and amphibolic tuff breccia are 17.1 ± 0.4, 17.5 ± 0.3, and 16.9 ± 0.3 Ma, respectively (Wu et al., 2015). The dating results indicate that the igneous rocks in Ciemas were all formed by the Middle Miocene magmatism (Wu et al., 2015; Zhang et al., 2015).

The geochemical characteristics of the Ciemas igneous rocks show that the quartz diorite porphyry belongs to the calc-alkaline to high potassium calc-alkaline series (Wu et al., 2015). The primitive mantle-normalized trace element patterns of all the rocks are similar, with relative enrichments in the large ion lithophile elements (LILE) Rb, Th, and U and relative depletions of the high field strength elements (HFSE) Nb, Ta, Zr, and Hf, which are similar to those of the typical arc magmatic rocks (Martin et al., 1999; Wu et al., 2015).

The zircons ε_{Hf} (t) of the Ciemas igneous rocks are consistent, with an average of −11.15 ± 0.39 (Table 1, Fig. 9d and 10), and the peak value of T_{DM2} is 1500–1650 Ma, which suggests the Middle Miocene arc magmatism in West Java experienced intense crustal contamination. Java is located in the southern border of Sundaland, indicating that the Middle Miocene (~17 Ma) magmatism in Ciemas may be contaminated by underlying Sundaland.

The elemental geochemistry and Hf isotopes of the igneous rock indicate that the Ciemas igneous rocks originated from the same arc magmatism event with intense crustal contamination. As the Indian-Australian Plate subducted beneath the Eurasian Plate, the addition of fluid from the dehydration of the subducted slab resulted in partial melting of the overlying mantle wedge and generated mafic magma (Wu et al., 2015). This magma evolved further in the crust and was contaminated by Sundaland, resulting in the Middle Miocene arc magmatism in the Ciemas area.

5.2. Contribution of continental crust for mineralization

The low-sulfidation epithermal deposits are mainly concentrated in West Java, which is coupled with the distribution of the Sundaland underlain in Java (Fig. 1B) (Hall, 2002; Maryono et al., 2018). This observation suggests that the Sundaland may contribute to the low-sulfidation epithermal mineralization in West Java.

The Pb isotopes of sulfides (galena, pyrite and arsenopyrite) are consistent with high radiogenic Pb (Fig. 11). The mean ratios of $^{206}Pb/^{204}Pb$, $^{207}Pb/^{204}Pb$ and $^{208}Pb/^{204}Pb$ are 39.343 ± 0.059, 15.730 ± 0.015 and 18.854 ± 0.025, respectively, indicating that the mineralization materials of the Ciemas gold deposit mainly originated from ancient continental crust (Table 2). These ratios are similar to the

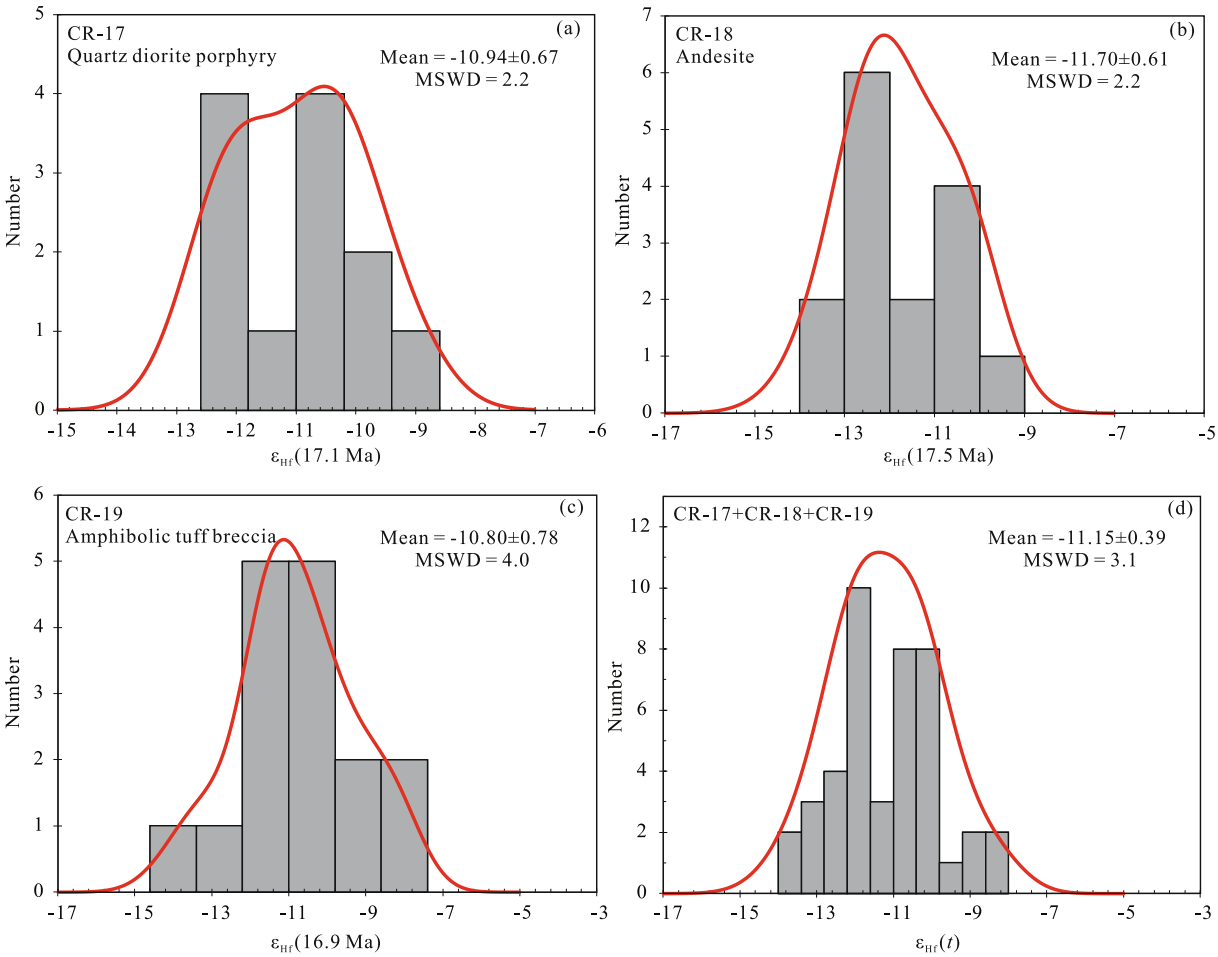

Fig. 9. Zircon Hf isotopic compositions of quartz diorite porphyry (a), andesite (b), amphibolic tuff breccia (c), and all the three samples (d) in Ciemas.

Pb isotopes of Pliocene volcanic rocks and sulfides of epithermal deposits but are different from Miocene volcanic rocks in the Bayah Dome (Fig. 11). The Pb isotopic compositions of the Pliocene volcanic rocks and the associated mineralization are very similar in Bayah Dome; $^{206}Pb/^{204}Pb$ ranges from 18.71 to 18.81 and from 18.74 to 18.80, respectively (Fig. 11) (Milési et al., 1999). The isotopic signature suggests that the mineralization and associated volcanic rocks both originated Sundaland that melted and remobilized during the Pliocene volcanism and hydrothermal events (Marcoux and Milési, 1994; Milési et al., 1999). The tin deposits in Indo-Chinese peninsula also have the similar Pb isotopic compositions ($^{206}Pb/^{204}Pb$ = 18.497 and 18.609) (Jones et al. 1977), which indicates continental basement beneath West Java may be similar to that exposed on the Indo-Chinese peninsula (Milési et al., 1999). Conversely, the barren Miocene volcanics in the Bayah Dome appear to be less dependent on the participation of this ancient crust (Marcoux and Milési, 1994; Milési et al., 1999). Their isotopic compositions ($^{206}Pb/^{204}Pb \sim 15.56$) indicate a mantle origin with slight crustal contamination, which is consistent with the isotopic compositions in lavas of mature island arcs (Fig. 11) (Doe and Zartman, 1979). Therefore, the ore-forming materials of Ciemas deposit mainly originated from the underlying Sundaland, which is similar to the epithermal mineralization in Bayah Dome.

5.3. Metallogenic events in Java

In East Java and its east, major porphyry deposits distributed from the Hu'u deposit in the east, through the Elang and Batu Hijau deposits in Sumbawa, the Selodong deposit in Lombok, and the Tumpangpitu deposit in East Java to the west (Fig. 1B) (Harrison et al., 2018; Maryono et al., 2018). To the west, the porphyry mineralization gradually decreased (Setijadji et al., 2006; Maryono et al., 2018). The typical porphyry deposits in Central and East Java, including the Tumpangpitu, Trenggalek and Selogiri, occur in the southern region (Fig. 1B). High-sulfidation epithermal deposits and prospects in this area are associated with porphyry deposits and occur at Tumpangpitu, Selogiri and Karangbolong (Fig. 1B) (Setijadji et al., 2006; Maryono et al., 2018). Metallogenic time ranges from 21.7 to 3.9 Ma (Setijadji et al., 2006). However, the giant deposits mainly formed less than 5 Ma (Maryono et al., 2018).

The low-sulfidation epithermal deposits occurred widespread along the southern part of Java (Fig. 1B). In West Java, many epithermal deposits clustered within the Bayah Dome (Fig. 1B). The Bayah Dome, located in the western part of the West Java, is exposed over an area of approximately 40 × 80 km (Milési et al., 1999). The volcanic rocks at the Bayah Dome complex mainly consist of the Late Miocene to Pliocene rhyolitic to andesitic rocks. The ages of those volcanic rocks are 14

Table 1
Zircon Lu-Hf isotopic compositions for igneous rocks in Ciemas.

Analysed point	$^{176}Hf/^{177}Hf$	1σ	$^{176}Lu/^{177}Hf$	1σ	$^{176}Yb/^{177}Hf$	1σ	Age (Ma)	εHf(0)	1σ	εHf(*t*)	1σ	T_{DM1}	T_{DM2}	$f_{Lu/Hf}$
Quartz diorite porphyry														
CR17-01	0.282418	0.000016	0.001561	0.000007	0.050343	0.000392	17.1	−12.5	0.8	−12.2	0.8	1196	1637	−0.95
CR17-02	0.282431	0.000013	0.001237	0.000009	0.038306	0.000280	17.1	−12.0	0.7	−11.7	0.7	1167	1611	−0.96
CR17-03	0.282419	0.000018	0.001477	0.000013	0.048430	0.000369	17.1	−12.5	0.8	−12.1	0.8	1192	1635	−0.96
CR17-04	0.282468	0.000015	0.001362	0.000014	0.042480	0.000507	17.1	−10.7	0.7	−10.4	0.7	1118	1539	−0.96
CR17-05	0.282469	0.000013	0.001325	0.000014	0.040746	0.000396	17.1	−10.7	0.7	−10.4	0.7	1117	1538	−0.96
CR17-06	0.282475	0.000013	0.000747	0.000020	0.023332	0.000588	17.1	−10.5	0.7	−10.1	0.7	1091	1525	−0.98
CR17-07	0.282413	0.000014	0.000989	0.000008	0.032075	0.000232	17.1	−12.7	0.7	−12.3	0.7	1185	1647	−0.97
CR17-08	0.282462	0.000013	0.001311	0.000020	0.040668	0.000701	17.1	−11.0	0.7	−10.6	0.7	1127	1552	−0.96
CR17-09	0.282480	0.000013	0.001414	0.000012	0.044458	0.000437	17.1	−10.3	0.7	−10.0	0.7	1103	1515	−0.96
CR17-10	0.282452	0.000013	0.000935	0.000017	0.029554	0.000584	17.1	−11.3	0.7	−10.9	0.7	1128	1570	−0.97
CR17-11	0.282504	0.000012	0.000620	0.000005	0.018773	0.000184	17.1	−9.5	0.7	−9.1	0.7	1047	1469	−0.98
CR17-12	0.282422	0.000014	0.000628	0.000005	0.019269	0.000149	17.1	−12.4	0.7	−12.0	0.7	1162	1630	−0.98
Andesite														
CR18-01	0.282420	0.000013	0.000655	0.000009	0.020030	0.000228	17.5	−12.4	0.7	−12.1	0.7	1165	1633	−0.98
CR18-02	0.282433	0.000012	0.000582	0.000003	0.018227	0.000108	17.5	−12.0	0.7	−11.6	0.7	1145	1608	−0.98
CR18-03	0.282475	0.000013	0.001048	0.000006	0.031996	0.000222	17.5	−10.5	0.7	−10.1	0.7	1100	1525	−0.97
CR18-04	0.282411	0.000015	0.001492	0.000036	0.048421	0.001372	17.5	−12.8	0.7	−12.4	0.7	1204	1651	−0.96
CR18-05	0.282480	0.000017	0.001191	0.000015	0.037709	0.000466	17.5	−10.3	0.8	−9.9	0.8	1096	1515	−0.96
CR18-06	0.282472	0.000016	0.001203	0.000020	0.037148	0.000442	17.5	−10.6	0.8	−10.3	0.8	1109	1532	−0.96
CR18-07	0.282452	0.000014	0.001088	0.000013	0.035424	0.000643	17.5	−11.3	0.7	−10.9	0.7	1133	1570	−0.97
CR18-08	0.282399	0.000016	0.001457	0.000024	0.048653	0.000915	17.5	−13.2	0.8	−12.8	0.8	1219	1673	−0.96
CR18-09	0.282417	0.000015	0.000975	0.000016	0.032001	0.000582	17.5	−12.6	0.7	−12.2	0.7	1179	1639	−0.97
CR18-10	0.282386	0.000015	0.002060	0.000087	0.071141	0.003326	17.5	−13.6	0.7	−13.3	0.7	1258	1699	−0.94
CR18-11	0.282409	0.000014	0.001003	0.000010	0.031801	0.000377	17.5	−12.8	0.7	−12.5	0.7	1191	1654	−0.97
CR18-12	0.282413	0.000015	0.001408	0.000006	0.044048	0.000169	17.5	−12.7	0.7	−12.3	0.7	1198	1646	−0.96
CR18-13	0.282376	0.000021	0.004179	0.000114	0.136948	0.003567	17.5	−14.0	0.9	−13.7	0.9	1351	1720	−0.87
CR18-14	0.282445	0.000015	0.001209	0.000018	0.037545	0.000727	17.5	−11.6	0.7	−11.2	0.7	1147	1584	−0.96
CR18-15	0.282453	0.000016	0.001648	0.000007	0.053879	0.000268	17.5	−11.3	0.8	−10.9	0.8	1149	1569	−0.95
Amphibolic tuff breccia														
CR19-01	0.282433	0.000014	0.000949	0.000002	0.031532	0.000062	16.9	−12.0	0.7	−11.6	0.7	1156	1607	−0.97
CR19-02	0.282486	0.000014	0.001101	0.000010	0.034891	0.000407	16.9	−10.1	0.7	−9.8	0.7	1086	1504	−0.97
CR19-03	0.282458	0.000014	0.001176	0.000008	0.038596	0.000314	16.9	−11.1	0.7	−10.7	0.7	1128	1559	−0.96
CR19-04	0.282435	0.000015	0.000693	0.000007	0.023713	0.000250	16.9	−11.9	0.7	−11.6	0.7	1145	1604	−0.98
CR19-05	0.282520	0.000016	0.001312	0.000014	0.042240	0.000500	16.9	−8.9	0.8	−8.6	0.8	1044	1438	−0.96
CR19-06	0.282430	0.000014	0.000609	0.000007	0.019771	0.000342	16.9	−12.1	0.7	−11.7	0.7	1150	1613	−0.98
CR19-07	0.282454	0.000015	0.000809	0.000013	0.026682	0.000468	16.9	−11.2	0.7	−10.9	0.7	1122	1567	−0.98
CR19-08	0.282429	0.000015	0.001514	0.000015	0.049909	0.000581	16.9	−12.1	0.7	−11.8	0.7	1179	1616	−0.95
CR19-09	0.282480	0.000014	0.001306	0.000004	0.042195	0.000178	16.9	−10.3	0.7	−10.0	0.7	1101	1517	−0.96
CR19-10	0.282465	0.000014	0.000823	0.000007	0.026738	0.000242	16.9	−10.9	0.7	−10.5	0.7	1108	1545	−0.98
CR19-11	0.282504	0.000014	0.000982	0.000006	0.029618	0.000173	16.9	−9.5	0.7	−9.1	0.7	1057	1468	−0.97
CR19-12	0.282532	0.000014	0.000891	0.000023	0.027611	0.000736	16.9	−8.5	0.7	−8.1	0.7	1016	1415	−0.97
CR19-13	0.282374	0.000018	0.002139	0.000019	0.073446	0.000677	16.9	−14.1	0.8	−13.7	0.8	1278	1723	−0.94
CR19-14	0.282439	0.000013	0.001317	0.000015	0.041101	0.000443	16.9	−11.8	0.7	−11.4	0.7	1159	1597	−0.96
CR19-15	0.282462	0.000015	0.000708	0.000011	0.021666	0.000328	16.9	−11.0	0.7	−10.6	0.7	1109	1551	−0.98
CR19-16	0.282393	0.000014	0.001365	0.000042	0.047754	0.001684	16.9	−13.4	0.7	−13.1	0.7	1225	1686	−0.96

Notes: The weighted average ages of zircons are used for calculations of the $\varepsilon_{Hf}(t)$ and the T_{2DM}.
Parameters: $(^{176}Hf/^{177}Hf)^{0}_{CHUR} = 0.282772 \pm 0.000029$, $(^{176}Lu/^{177}Hf)^{0}_{CHUR} = 0.0332 \pm 0.0002$ (Blichert-Toft and Albarède, 1997); $(^{176}Hf/^{177}Hf)^{0}_{DM} = 0.28325$, $(^{176}Lu/^{177}Hf)^{0}_{DM} = 0.0384$, $f_{DM} = 0.16$ (Griffin et al., 2000), $f_{BBC} = -0.65$ (Rudnick and Gao, 2003). Decay constant: $\lambda = 1.867 \times 10^{-11}\ y^{-1}$ (Söderlund et al., 2004); calculation formula: $\varepsilon_{Hf}(t) = [(^{176}Hf/^{177}Hf)^{t}_{spl}/(^{176}Hf/^{177}Hf)^{t}_{CHUR} - 1] \times 10^{4}$, $(^{176}Hf/^{177}Hf)^{t} = (^{176}Hf/^{177}Hf)^{0} - (^{176}Lu/^{177}Hf)^{0}\ (e^{\lambda t} - 1)$, $T_{DM1} = 1/\lambda \ln\{[(^{176}Hf/^{177}Hf)\ 0s_{pl} - (^{176}Hf/^{177}Hf)^{0}_{DM}]/[(^{176}Lu/^{177}Hf)^{0}_{spl} - (^{176}Lu/^{177}Hf)^{0}_{DM}] + 1$, $T_{DM2} = T_{DM1} - (T_{DM1} - f_{spl}) \times (f_{BBC} - f_{spl})/(f_{BBC} - f_{DM})$.

to 2 Ma, as revealed by K-Ar dating (Marcoux and Milési, 1994). Typical deposits include the Cirotan, Cikotok, Cipanglengseran, Pongkor, Ciawitali and Cikidang (Fig. 1B). These ore-forming ages are mainly concentrated in the Pliocene to Pleistocene (1.7–2.05 Ma) (Marcoux et al., 1993; Basuki et al., 1994; Marcoux and Milési, 1994; Milési et al., 1994; Milési et al., 1999).

In addition, some porphyry and epithermal Au (Ag) deposits have been found in the south of West Java, including the low-sulfidation Cibaliung Au-Ag deposit (ore-forming age: 10.7–11.2 Ma), the high-sulfidation Cijulang Au deposit, the Arinem Au-Ag deposit (8.8–9.4 Ma) with high-sulfidation mineralization overlying the low-sulfidation, the high-sulfidation Cineam Au-Ag deposit (8.5–9.6 Ma) and the porphyry-epithermal Ciemas Au deposit (~17 Ma) (Fig. 1B) (Harijoko et al., 2007; Tun et al., 2014; Yuningsih and Matsueda, 2014; Zhang et al., 2015). These mineralizations are mainly related to the Jampang Formation that was formed in the Early-Middle Miocene (23–11.6 Ma) (Yuningsih et al., 2012). The quartz vein and structure-controlled alternated ore blocks in Ciemas Au deposit occurred in the Jampang Formation, and the associated igneous yielded ~ 17 Ma (Wu et al., 2014; Zhang et al., 2015). Moreover, some epithermal and

Table 2
Pb isotopic compositions of sulfides in Ciemas.

Sample No.	$^{208}Pb/^{204}Pb$	1σ	$^{207}Pb/^{204}Pb$	1σ	$^{206}Pb/^{204}Pb$	1σ	$^{208}Pb/^{206}Pb$	1σ	$^{207}Pb/^{206}Pb$	1σ
C09a-Asp1	39.325	0.018	15.720	0.007	18.829	0.008	2.0884	0.0001	0.8348	0.0000
C09a-Asp2	39.425	0.075	15.770	0.030	18.896	0.035	2.0882	0.0003	0.8350	0.0001
C09a-Asp4	39.411	0.011	15.752	0.004	18.879	0.005	2.0877	0.0001	0.8345	0.0000
C09a-Asp5	39.273	0.037	15.710	0.015	18.809	0.018	2.0879	0.0002	0.8354	0.0001
C09a-Asp6	39.286	0.110	15.707	0.044	18.818	0.052	2.0876	0.0004	0.8349	0.0002
C09a-Asp7	39.370	0.015	15.735	0.006	18.850	0.007	2.0885	0.0001	0.8348	0.0000
C09a-Py1	39.307	0.064	15.718	0.025	18.820	0.029	2.0873	0.0002	0.8347	0.0001
C09a-Py2	39.329	0.033	15.729	0.013	18.845	0.015	2.0872	0.0001	0.8347	0.0001
C09a-Py3	39.317	0.005	15.718	0.002	18.836	0.002	2.0873	0.0000	0.8345	0.0000
C09a-Py4	39.230	0.034	15.700	0.013	18.790	0.016	2.0879	0.0001	0.8353	0.0001
C09a-Py5	39.307	0.025	15.723	0.010	18.827	0.012	2.0881	0.0001	0.8351	0.0001
C09a-Py6	39.317	0.062	15.723	0.025	18.834	0.029	2.0883	0.0002	0.8352	0.0001
C18b-Py2	39.180	0.012	15.717	0.004	18.827	0.005	2.0810	0.0001	0.8349	0.0000
C18b-Py3	39.194	0.013	15.728	0.005	18.823	0.006	2.0824	0.0001	0.8356	0.0000
C18b-Py5	39.367	0.005	15.733	0.002	18.853	0.002	2.0877	0.0001	0.8344	0.0000
CBT-11-Gn1	39.346	0.013	15.741	0.005	18.878	0.004	2.0845	0.0002	0.8340	0.0000
CBT-11-Gn2	39.334	0.012	15.742	0.004	18.875	0.004	2.0841	0.0001	0.8341	0.0000
CBT-11-Gn3	39.390	0.014	15.736	0.005	18.871	0.005	2.0875	0.0002	0.8340	0.0000
CBT-4-Gn1	39.373	0.012	15.731	0.004	18.865	0.004	2.0870	0.0002	0.8340	0.0000
CBT-4-Gn3	39.392	0.007	15.736	0.003	18.874	0.003	2.0870	0.0001	0.8338	0.0000
CBT-4-Gn4	39.389	0.005	15.734	0.002	18.874	0.002	2.0867	0.0001	0.8337	0.0000
CBT-4-Gn5	39.391	0.004	15.734	0.002	18.874	0.002	2.0867	0.0001	0.8337	0.0000
CBT-4-Py1	39.330	0.007	15.735	0.002	18.868	0.003	2.0845	0.0001	0.8340	0.0000
CBT-4-Py2	39.355	0.013	15.723	0.005	18.856	0.006	2.0871	0.0001	0.8338	0.0000
CBT-4-Py3	39.374	0.014	15.727	0.005	18.864	0.006	2.0873	0.0001	0.8338	0.0000
CBT-4-Py4	39.346	0.013	15.719	0.005	18.853	0.006	2.0870	0.0001	0.8338	0.0000
P5a-Gn1	39.390	0.005	15.736	0.002	18.874	0.002	2.0868	0.0001	0.8337	0.0000
P5a-Gn1	39.394	0.007	15.737	0.002	18.873	0.002	2.0873	0.0001	0.8338	0.0000
P5a-Gn2	39.380	0.006	15.733	0.002	18.868	0.002	2.0872	0.0001	0.8339	0.0000
P5a-Gn4	39.357	0.004	15.726	0.002	18.859	0.002	2.0869	0.0001	0.8339	0.0000
P5a-Py1	39.396	0.005	15.738	0.002	18.871	0.002	2.0875	0.0001	0.8340	0.0000
P5a-Py3	39.361	0.019	15.721	0.007	18.859	0.009	2.0875	0.0001	0.8339	0.0000
P5a-Py5	39.374	0.011	15.732	0.004	18.861	0.005	2.0876	0.0001	0.8340	0.0000

Notes: C – sample from the Cibak ore block; CBT – sample from the Cibatu ore block; P- sample from the Pasir Manggu ore block; Asp – Arsenopyrite; Py – Pyrite; Gn – Galena.

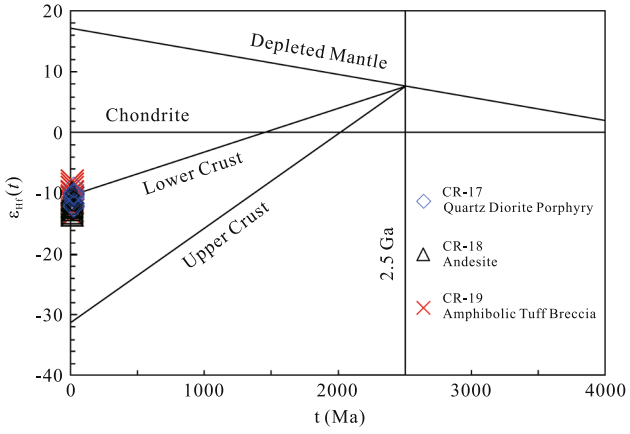

Fig. 10. Zircon Hf isotopic compositions verses ages for quartz diorite porphyry, andesite and amphibolic tuff breccia in Ciemas.

volcanogenic massive sulfide (VMS) deposits associated with the Jampang Formation have been discovered in Cianjur (Gunung Subang) and Tasikmalaya (Ciasah-Cidadap-Cibuniasih) districts in West Java (JICA-JOGMEC, 1996; Setijadji et al., 2006; Sunarie et al, 2009), which indicates that an important metallogenic event occurred in West Java during Miocene. The origins of this metallogenic event and associated magmatism may be closely related the underlying Sundaland, which is similar to that in the Ciemas area.

6. Conclusions

The zircons ε_{Hf} (t) of the igneous rocks in Ciemas are consistent, with an average of -11.15 ± 0.39, and the peak value of T_{DM2} is 1500–1650 Ma, which suggests the Sundaland participated in the Middle Miocene arc magmatism in Ciemas.

The *in situ* Pb isotopic compositions of sulfides are very uniform and have high radiogenic lead in the Ciemas Au deposit, indicating that the metallogenic materials of the Ciemas gold deposit mainly originate from underlying Sundaland.

The multistage arc magmatism induced by the subduction of Indian-Australian Plate northward beneath Java Island controls the porphyry and epithermal mineralization in Java. There is an important metallogenic event in West Java during Miocene, except Pliocene-Pleistocene porphyry mineralization in East Java and low-sulfidation mineralization in West Java.

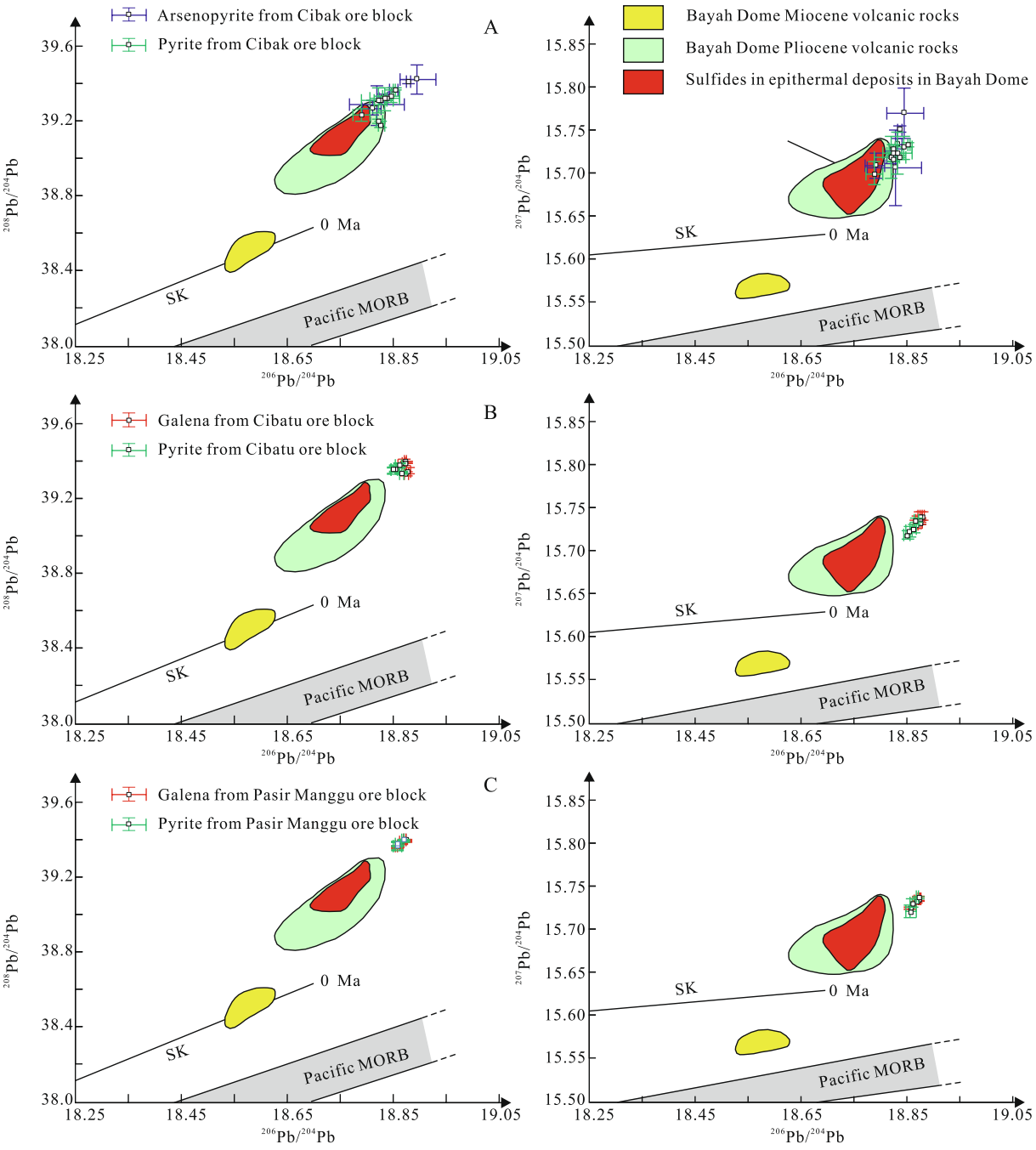

Fig. 11. Lead-isotope diagrams of sulfides in Ciemas, west Java. SK: evolution curve from (Stacey and Kramers, 1975); Pb isotope data of Miocene and Pliocene volcanic rocks and sulfides of epithermal deposits in the Bayah Dome from (Marcoux and Milési, 1994; Milési et al., 1994; Milési et al., 1999).

Acknowledgements

The research was financially supported by the Natural Science Foundation of China (NSFC Nos. 41573039, U1603245, 41703051 and U1812402), the Chinese Academy of Sciences "Light of West China" Program and the Natural Science Foundation of Guizhou Province (No. [2018] 1171). Mr. Wijaya Lawrence and Mr. Haifeng Wang from PT. WILTON WAHANA INDONESIA company provided much support for fieldtrips.

References

Angeles, C.A., Prihatmoko, S., Walker, J.S., 2002. Geology and alteration-mineralization characteristics of the Cibaliung epithermal gold deposit, Banten, Indonesia. Resour. Geol. 52 (4), 329–339.
Audley-Charles, M., Ballantyne, P., Hall, R., 1988. Mesozoic-Cenozoic rift-drift sequence of Asian fragments from Gondwanaland. Tectonophysics 155 (1), 317–330.
Bao, Z.A., Chen, L., Zong, C.L., Yuan, H.L., Chen, K.Y., Dai, M.N., 2017. Development of pressed sulfide powder tablets for in situ sulfur and lead isotope measurement using LA-MC-ICP-MS. Int. J. Mass Spectrom. 421, 255–262.
Basuki, A., Sumanagara, D.A., Sinambela, D., 1994. The Gunung Pongkor gold-silver deposit, West Java, Indonesia. J. Geochem. Explor. 50 (1–3), 371–391.
Bemmelen, R.W., 1949. The Geology of INDONESIA. 1. US Government Printing Office.
Bemmelen, R.W., 1970. The Geology of Indonesia. Martinus Nijhoff, The Hague, pp. 732.
Ben-Avraham, Z., Emery, K.O., 1973. Structural framework of Sunda Shelf. Bull. Am. Assoc. Pet. Geol. 57 (12), 2323–2366.
Blichert-Toft, J., Albarède, F., 1997. The Lu-Hf isotope geochemistry of chondrites and the evolution of the mantle-crust system. Earth Planet. Sci. Lett. 148 (1–2), 243–258.
Carlile, J.C., Mitchell, A.H.G., 1994. Magmatic arcs and associated gold and copper mineralization in Indonesia. J. Geochem. Explor. 50 (50), 91–142.
Clements, B., Hall, R., 2007. Cretaceous to late Miocene stratigraphic and tectonic evolution of West Java. Proceedings, Indonesian Petroleum Association. Thirty-First

Annual Convention and Exhibition, IPA07-G-037.
Doe, B., Zartman, R., 1979. Plumbotectonics, the phanerozoic. In: Barnes, H.L. (Ed.), Geochemistry of Hydrothermal Ore Deposits, 2nd ed. John Wiley and Sons, New-York, pp. 22–70.
Elburg, M., Van Bergen, M., Foden, J., 2004. Subducted upper and lower continental crust contributes to magmatism in the collision sector of the Sunda-Banda arc, Indonesia. Geology 32 (1), 41–44.
Griffin, W., Pearson, N., Belousova, E., Jackson, S.v., Van Achterbergh, E., O'Reilly, S.Y., Shee, S., 2000. The Hf isotope composition of cratonic mantle: LAM-MC-ICPMS analysis of zircon megacrysts in kimberlites. Geochim. Cosmochim. Acta 64 (1), 133–147.
Hall, R., 2002. Cenozoic geological and plate tectonic evolution of SE Asia and the SW Pacific: computer-based reconstructions, model and animations. J. Asian Earth Sci. 20 (4), 353–431.
Hall, R., Hattum, M.W.A.V., Spakman, W., 2008. Impact of India-Asia collision on SE Asia: the record in Borneo. Tectonophysics 451 (1–4), 366–389.
Hamilton, W., 1973. Tectonics of the Indonesian Region. Geol. Soc. Malaysia, Bull. 6, 3–10.
Hamilton, W., 1989. Convergent-plate tectonics viewed from the Indonesia region. Geol. Indonesia 12, 35–88.
Hamilton, W.B., 1979. Tectonics of the Indonesian region. United States Government. Printing Office.
Harijoko, A., Ohbuchi, Y., Motomura, Y., Imai, A., Watanabe, K., 2007. Characteristics of the cibaliung gold deposit: miocene low-sulfidation-type epithermal gold deposit in Western Java, Indonesia. Resour. Geol. 57 (2), 114–123.
Harijoko, A., Sanematsu, K., Duncan, R.A., Prihatmoko, S., Watanabe, K., 2004. Timing of the mineralization and volcanism at Cibaliung gold deposit, western Java, Indonesia. Resour. Geol. 54 (2), 187–195.
Harrison, R.L., Maryono, A., Norris, M.S., Rohrlach, B.D., Cooke, D.R., Thompson, J.M., Creaser, R.A., Thiede, D.S., 2018. Geochronology of the Tumpangpitu porphyry Au-Cu-Mo and high-sulfidation epithermal Au-Ag-Cu deposit: evidence for pre-and postmineralization diatremes in the Tujuh Bukit district, Southeast Java, Indonesia. Econ. Geol. 113 (1), 163–192.
Hu, Z., Liu, Y., Gao, S., Liu, W., Zhang, W., Tong, X., Lin, L., Zong, K., Li, M., Chen, H., 2012a. Improved in situ Hf isotope ratio analysis of zircon using newly designed X skimmer cone and jet sample cone in combination with the addition of nitrogen by laser ablation multiple collector ICP-MS. J. Anal. At. Spectrom. 27 (9), 1391–1399.
Hu, Z., Liu, Y., Gao, S., Xiao, S., Zhao, L., Günther, D., Li, M., Zhang, W., Zong, K., 2012b. A "wire" signal smoothing device for laser ablation inductively coupled plasma mass spectrometry analysis. Spectrochim. Acta, Part B 78, 50–57.
Imai, A., Watanabe, K., 2007. Origin of ore-forming fluids responsible for gold mineralization of the Pongkor Au-Ag Deposit, West Java, Indonesia: evidence from mineralogic, fluid inclusion microthermometry and stable isotope study of the Ciurug-Cikoret veins. Resour. Geol. 57 (2), 136–148.
Indarto, S., Sudarsono, Setiawan, I., 2006. Genetic model of hydrothermal mineralization in the Cupunagara area, Subang, West Java. In: Conference Proceeding "Opportunities and Roles of Earth Sciences in Sustainable Development". LIPI Geotechnology Research Center, pp. 231–242 (in Indonesia).
Ismayanto, A.F., Setiawan, I., Sumantri, Toto, Listiyowati, A.F., 2007. Hydrothermal Mineralization Model in the Southern Java Mountains: Case of the Gunung Subang area, Tanggeung District, Cianjur, West Java. Internal Research Report. LIPI Geotechnology Research Center (in Indonesia).
Jonathan, M.N., 2007. Ciemas prospect West Java, Indonesia geological evaluation study. Jakarta: Geological Report, pp. 1–46.
Jones, M., Reed, B., Doe, B., Lanphere, M., 1977. Age of tin mineralization and plumbotectonics, Belitung, Indonesia. Econ. Geol. 72 (5), 745–752.
Japan International Corporation Agency-Japan Oil, G., Metal National Corporation (JICA-JOGMEC), 1996. Report on the Cooperative Mineral Exploration in the Tasikmalaya Area, West Java, Phase 2, Japan International Corporation Agency and Japan Oil, Gas, Metal National Corporation, Tokyo.
Katili, J.A., 1975. Volcanism and plate tectonics in the Indonesian island arcs. Tectonophysics 26 (3), 165–188.
Katili, J.A., 1978. Past and present geotectonic position of Sulawesi, Indonesia. Tectonophysics 45 (4), 289–322.
Kisman, 2011. Arsenic (As) as an Indicator Element for Epithermal Type Gold Mineralization in the Area of Cisolok, Sukabumi Regency, West Java. Buletin Sumber Daya Geologi 6 (1), 23–32 in Indonesia.
Liu, Y., Gao, S., Hu, Z., Gao, C., Zong, K., Wang, D., 2010. Continental and oceanic crust recycling-induced melt–peridotite interactions in the Trans-North China Orogen: U-Pb dating, Hf isotopes and trace elements in zircons from mantle xenoliths. J. Petrol. 51 (1–2), 537–571.
Malod, J., Karta, K., Beslier, M., Zen Jr, M., 1995. From normal to oblique subduction: Tectonic relationships between Java and Sumatra. J. SE Asian Earth Sci. 12 (1), 85–93.
Marcoux, E., Milési, J.-P., 1994. Epithermal gold deposits in West Java, Indonesia: geology, age and crustal source. J. Geochem. Explor. 50 (1), 393–408.
Marcoux, E., Milési, J., Sohearto, S., Rinawan, R., 1993. Noteworthy mineralogy of the Au-Ag-Sn-W (Bi) epithermal ore deposit of Cirotan, West Java, Indonesia. Canad. Mineral. 31 (3), 727–744.
Martin, H., Sial, A.N., Stephens, W.E., Ferreira, V.P., 1999. Adakitic magmas; modern analogues of Archaean granitoids. Lithos 46 (3), 411–429.
Maryono, A., Harrison, R.L., Cooke, D.R., Rompo, I., Hoschke, T.G., 2018. Tectonics and geology of porphyry Cu-Au deposits along the eastern Sunda magmatic arc, Indonesia. Econ. Geol. 113 (1), 7–38.
Metcalfe, I., 1996. Pre-Cretaceous evolution of SE Asian terranes. In: Hall, R., Blundell, D.J. (Eds.), Tectonic Evolution of SE Asia. Geological Society London Special Publications, pp. 97–122.
Milési, J., Marcoux, E., Nehlig, P., Sunarya, Y., Sukandar, A., Felenc, J., 1994. Cirotan, West Java, Indonesia; a 1.7 Ma hybrid epithermal Au-Ag-Sn-W deposit. Econ. Geol. 89 (2), 227–245.
Milési, J., Marcoux, E., Sitorus, T., Simandjuntak, M., Leroy, J., Bailly, L., 1999. Pongkor (west Java, Indonesia): a pliocene supergene-enriched epithermal Au-Ag-(Mn) deposit. Miner. Deposita 34 (2), 131–149.
Miyazaki, K., Sopaheluwakan, J., Zulkarnain, I., Wakita, K., 1998. A jadeite–quartz–glaucophane rock from Karangsambung, central Java, Indonesia. Island Arc 7 (1–2), 223–230.
Nicholls, I., Whitford, D., Harris, K., Taylor, S., 1980. Variation in the geochemistry of mantle sources for tholeiitic and calc-alkaline mafic magmas, western Sunda volcanic arc, Indonesia. Chem. Geol. 30 (3), 177–199.
Prabowo, S.A., Rosana, M.F., Haryanto, A.D., 2018. Relationship between Au-Ag high grade ore mineralization zone at Cijiwa epithermal vein system, Simpenan sub-district, Sukabumi district, West Java Province. Padjadjaran Geosci. J. 2 (2), 139–144 (in Indonesia).
Rosana, M., Haryanto, A., Yuniardi, Y., Yuningsih, E., 2006. The occurrences of base metal Mineralization in Cikadu-Cisungsang area, Banten Province, Indonesia. Prosiding Persidangan Bersama Geosains ITB-UKM 164–166.
Rosana, M., Matsueda, H., 2002a. First observation of the base metal mineralization in the Cikidang gold mining area, Western Java, Indonesia. Resource Geol. Ann. Meet 52, p03.
Rosana, M.F., Matsueda, H., 2002b. Cikidang hydrothermal gold deposit in western Java, Indonesia. Resour. Geol. 52 (4), 341–352.
Rudnick, R.L., Gao, S., 2003. Composition of the continental Crust. In: Rudnick, R.L. (Ed.), Treatise on geochemistry. Elsevier, pp. 1–64 659.
Setijadji, L.D., Kajino, S., Imai, A., Watanabe, K., 2006. Cenozoic island arc magmatism in Java Island (Sunda Arc, Indonesia): clues on relationships between geodynamics of volcanic centers and ore mineralization. Resour. Geol. 56 (3), 267–292.
Smyth, H., Hamilton, P., Hall, R., Kinny, P., 2007. The deep crust beneath island arcs: inherited zircons reveal a Gondwana continental fragment beneath East Java, Indonesia. Earth Planet. Sci. Lett. 258 (1), 269–282.
Soeria-Atmadja, R., Maury, R., Bellon, H., Pringgoprawiro, H., Polve, M., Priadi, B., 1994. Tertiary magmatic belts in Java. J. SE Asian Earth Sci. 9 (1), 13–27.
Söderlund, U., Patchett, P.J., Vervoort, J.D., Isachsen, C.E., 2004. The 176 Lu decay constant determined by Lu–Hf and U-Pb isotope systematics of Precambrian mafic intrusions. Earth Planet. Sci. Lett. 219 (3), 311–324.
Stacey, J.S., Kramers, J.D., 1975. Approximation of terrestrial lead isotope evolution by a 2-stage model. Earth Planet. Sci. Lett. 26 (2), 207–221.
Sukamto, R., 1975. Geologic Map of the Jampang and Balekambang quadrangles, Java 1: 100,000. Geological Research and Development Centre, Bandung.
Sunarie, C.Y., Rosana, M.F., Watanabe, K., Imai, A., 2009. Characteristics of Epithermal Gold Mineralization in Tanggeung Area, Cianjur, West Java, Indonesia. Proc. Int. Symp. Earth Sci. Technol. 2009, 403–407.
Tun, M.M., Warmada, I.W., Idrus, A., Harijoko, A., Verdiansyah, O., Watanabe, K., 2014. High sulfidation epithermal mineralization and ore mineral assemblages of Cijulang prospect, West Java, Indonesia. J. Southeast Asian Appl. Geol. 6 (1), 29–38.
Wakita, K., Metcalfe, I., 2005. Ocean plate stratigraphy in East and Southeast Asia. J. Asian Earth Sci. 24 (6), 679–702.
Warmada, I.W., Lehmann, B., Simandjuntak, M., Hemes, H.S., 2007. Fluid Inclusion, rare-earth element and stable isotope study of carbonate minerals from the Pongkor epithermal gold-silver deposit, West Java, Indonesia. Resour. Geol. 57 (2), 124–135.
Whitford, D., Nicholls, I., Taylor, S., 1979. Spatial variations in the geochemistry of Quaternary lavas across the Sunda arc in Java and Bali. Contrib. Miner. Petrol. 70 (3), 341–356.
Widi, B.N., Matsueda, H., 1998. Epithermal gold-silver-tellurides deposit of Cineam, tasikmalaya, District, West Java, Indonesia. Direct. Min. Resour. Indonesia Special Publ. 96, 1–19.
Wu, C.Q., Zhang, Z.W., Zheng, C.F., Yao, J.H., 2015. Mid-Miocene (~ 17 Ma) quartz diorite porphyry in Ciemas, West Java, Indonesia, and its geological significance. Int. Geol. Rev. 57 (9–10), 1294–1304.
Wu, C., Zhang, Z., Yang, X., Zheng, C., 2014. Geological and geochemical constraints on the trinity pattern of Au deposits in Ciemas West Java, Indonesia. Acta Geol. Sin. 88 (Supp. 2), 807–808.
Yao, H.Z., Zhu, Z.X., Wei, Y.G., Yang, Z.Q., Wu, J.H., 2010. In: Geology and Minerals of the Sunda-new Guinea Region. Geological publishing house, Beijing, pp. 1–277 in Chinese.
Yuan, H.L., Liu, X., Chen, L., Bao, Z., Chen, K.Y., Zong, C.L., Li, X.C., Qiu, J.W., 2018. Simultaneous measurement of sulfur and lead isotopes in sulfides using nanosecond laser ablation coupled with two multi-collector inductively coupled plasma mass spectrometers. J. Asian Earth Sci. 154, 386–396.
Yuningsih, E.T., Matsueda, H., 2014. Genesis and origin of Te–bearing gold–silver–base metal mineralization of the Arinem deposit in western Java, Indonesia. J. Mineral. Petrol. Sci. 109 (2), 49–61.
Yuningsih, E.T., Matsueda, H., Rosana, M.F., 2014. Epithermal gold-silver deposits in Western Java, Indonesia: gold-silver selenide-telluride mineralization. Indonesian J. Geosci. 1 (2), 71–81.
Yuningsih, E.T., Matsueda, H., Setyaraharja, E.P., Rosana, M.F., 2012. The Arinem Te-bearing gold-silver-base metal deposit, West Java, Indonesia. Resour. Geol. 62 (2), 140–158.
Zhang, Z., Wu, C., Yang, X., Zheng, C., Yao, J., 2015. The trinity pattern of Au deposits

with porphyry, quartz–sulfide vein and structurally-controlled alteration rocks in Ciemas, West Java, Indonesia. Ore Geol. Rev. 64, 152–171.
Zheng, C.F., Zhang, Z.W., Wu, C.Q., Yao, J.H., 2014a. Sulfur Isotope Composition of Ciemas Gold Deposit in West Java, Indonesia. Acta Geol. Sin. 88 (Supp. 2), 852–853.
Zheng, C.F., Zhang, Z.W., Wu, C.Q., Yao, J.H., 2014b. Study of fluid inclusions and its indication of the genetic type and gold precipitation of the Ciemas gold deposit, Indonesia. Acta Mineral. Sin. 34 (4), 581–590 (in Chinese with English abstract).
Zheng, C.F., Zhang, Z.W., Wu, C.Q., Yao, J.H., 2017. Genesis of the Ciemas gold deposit and relationship with epithermal deposits in West Java, Indonesia: constraints from fluid inclusions and stable isotopes. Acta Geol. Sin. 91 (3), 1025–1040.